Bioactive Materials 4 (2019) 303–311

Contents lists available at ScienceDirect

Bioactive Materials

journal homepage: http://www.keaipublishing.com/biomat

Effect of thermomechanical treatment on the mechanical and microstructural evolution of a β-type Ti-40.7Zr–24.8Nb alloy

Sertan Ozan[a,b,**], Jixing Lin[c], Weijie Weng[a], Yaowu Zhang[a], Yuncang Li[a], Cuie Wen[a,*]

[a] School of Engineering, RMIT University, Bundoora, Victoria, 3083, Australia
[b] Department of Mechanical Engineering, Yozgat Bozok University, 66100, Yozgat, Turkey
[c] Advanced Material Research and Development Center, Zhejiang Industry & Trade Vocational College, Wenzhou, Zhejiang, 325003, China

ARTICLE INFO

Keywords:
TZN (Ti–Nb–Zr) alloy
Orthopedic implants
Thermomechanical process
Deformation mechanism
Mechanical properties

ABSTRACT

In this study, the microstructural evolution and mechanical properties of a newly developed Ti-40.7Zr–24.8Nb (TZN) alloy after different thermomechanical processes were examined. As-cast TZN alloy plates were solution-treated at 890 °C for 1 h, after which the thickness of the alloy plates was reduced by cold rolling at reduction ratios of 20%, 56%, 76%, and 86%. Stress-induced α" formation, {332} < 113 > β mechanical twinning, and kink band formation were observed in the cold-rolled TZN alloy samples. In the TZN sample after cold rolling at the 86% reduction ratio plus a recrystallization annealing at 890 °C for 1 h, the deformation products of a stress-induced α" phase, {332} < 113 > β mechanical twinning, and kink bands disappeared, resulting in a fine, equiaxed single β phase. The alloy samples exhibited elongation at rupture ranging from 7% to 20%, Young's modulus ranging from 63 to 72 GPa and tensile strength ranging from 753 to 1158 MPa. The TZN alloy sample after cold rolling and recrystallization annealing showed a yield strength of 803 MPa, a tensile strength of 848 MPa, an elongation at rupture of 20%, and an elastic admissible strain of 1.22%, along with the most ductile fractures during tensile testing.

1. Introduction

Orthopedic implants are implanted into the human body in order to assist with carrying out the normal functions of the bone tissues and the joints and, as reported elsewhere [1–5], the implant materials may have to be removed if they are not comprised of biocompatible alloying elements. Nickel (Ni) is an alloying element that results in the most frequent allergic reactions among all alloying elements used in implant materials [6]. Revision surgery may be required, especially when an alloy containing Ni is implanted into patients who display allergic reactions to Ni [2,3]. Such revision surgery increases costs and forces patients to undergo a second surgery, which is an undesirable situation [7]. Thus, it is crucial that the implant materials are comprised of biocompatible alloying elements [7,8]. In addition to biological compatibility, mechanical compatibility is another factor that can minimize the need for revision surgery [7,9]. Balanced biological load distribution between the bone and the implant cannot occur where the Young's modulus of the implant material is higher than that of the bone tissue [10]. If a material that is much more rigid than bone is used, the rigid implant material carries the majority of the physiological load, resulting in an excessive difference in load distribution between the implant and the surrounding bone [10]. Hence stress shielding occurs, resulting in implant loosening due to bone resorption and atrophy, which is also undesirable [11].

Ti-40.7Zr–24.8Nb (wt.% hereafter) (TZN) is a newly developed β-type titanium (Ti) alloy with excellent biocompatibility and promising mechanical properties for biomedical applications [12]. The TZN alloy showed a tensile strength (σ_{ts}) of 704 MPa, a Young's modulus (E) of 63 GPa, and an elongation at rupture (ε) of 10% in the as-casted state [12]. Further improvement in the mechanical properties of TZN is important for achieving long service life with a TZN alloy implant. The mechanical performance indicators for orthopedic implant materials are defined as high mechanical strength, low Young's modulus, and high ductility [12–14]. Hence, it is necessary to keep the Young's modulus of the TZN alloy almost constant with further increases in mechanical strength and ductility. As reported elsewhere [13,14], thermomechanical processes can be considered as a promising approach in achieving enhanced strength and ductility without increasing

Peer review under responsibility of KeAi Communications Co., Ltd.
* Corresponding author.
** Corresponding author. School of Engineering, RMIT University, Bundoora, Victoria, 3083, Australia.
E-mail addresses: sertan.ozan@bozok.edu.tr (S. Ozan), cuie.wen@rmit.edu.au (C. Wen).

https://doi.org/10.1016/j.bioactmat.2019.10.007
Received 28 August 2019; Received in revised form 15 October 2019; Accepted 17 October 2019
Available online 25 October 2019

the Young's modulus.

Based on their room temperature microstructure, Ti alloys are classified as α, near α, α + β, metastable β, and stable β alloys [15]. The microstructure of Ti alloys can be modified via cold-forming [13,14,16–18], hot-forming [19,20], and heat-treatment procedures [13–15]. The capabilities of β Ti alloys modified by cold-forming are good [21]. It is well known that the surface qualities of parts obtained after cold forming are much better than those obtained by other processes, which is beneficial for reducing production costs. However, while an increase in mechanical strength is achieved as a result of cold forming, ductility worsens.

Different from other metallic materials, the deformation products (e.g. ω, and α") of metastable β-type Ti alloys that are generated during plastic deformation may change their Young's modulus [13,14,22,23]. The level at which the plastic deformation is applied also affects the deformation mechanisms and deformation products, leading to a change to the Young's modulus [13,14].

Another important aspect is that the TZN alloy contains high amounts of zirconium (Zr). The assimilation of a removable implant with the bone due to the precipitation of calcium phosphate on its surface is not desirable because this may cause refracturing of the bone during the removal of the implant [24,25]. The probability of the formation of new bone fractures when removing an implant is minimized if the bone and the implant material are not assimilated, and this also makes the removal of the implant easier after recovery [24]. It has been reported that Zr can effectively prevent the precipitation of calcium phosphate [24–26]; thus a TZN alloy with high Zr content (40.7 % wt.) can be anticipated to be a promising candidate for removable implant applications.

In this study, the effects of solution-treatment, cold-rolling, and recrystallization-annealing procedures on the microstructure and mechanical properties of the TZN alloy are examined. After recrystallization annealing, TZN shows a unique combination of good mechanical properties.

2. Experimental procedure

2.1. Materials preparation

Ingots of the TZN alloy with a composition of Ti-40.7Zr–24.8Nb (wt. %) was prepared via cold-crucible levitation melting. The ingots were re-melted five times in order to guarantee their chemical homogeneity. A solution treatment at 890 °C for 1 h was carried out on the TZN ingots before further cold rolling, and cold rolling plus recrystallization annealing. The alloy plates were then cold-rolled at different reduction ratios of 20%, 56%, 76%, and 86%. The solution-treated samples are referred to as TZN-S, and the samples after cold rolling at 20%, 56%, 76%, and 86% reduction ratios are referred to as TZN-A, TZN-B, TZN-C and TZN-D, respectively. The samples after cold rolling at the 86% reduction rate were subsequently subjected to recrystallization annealing at 890 °C for 1 h and this group of samples is referred to as TZN-R. The preparation steps of the thermomechanical processes for the TZN alloy samples are shown in Fig. 1.

Disc samples with dimensions of 8 mm and thickness of 2 mm were cut from the TZN alloy plates using electrical discharge machining (EDM) for microstructural analysis. The disc samples were ground using SiC grinding papers of up to 4000 grit, and polished to a mirror finish with an H_2O_2 and colloidal silica mixture solution. The microstructures of the samples were examined using optical microscopy (OM) and scanning electron microscopy (SEM) in electron backscatter diffraction (EBSD) mode. X-ray diffraction (XRD) (Bruker D8 Advance) was used to determine the phase constitutions of the samples using a Cu Kα radiation source under 40 kV and 40 mA operating conditions.

2.2. Mechanical property testing

Tensile samples of the TZN alloy plates were cut using EDM parallel to the rolling direction. The surfaces of the tensile samples were ground using SiC grinding paper up to 2400 grit. Tensile tests were performed at a strain rate of $1 \times 10^{-3}\,s^{-1}$ at room temperature using a video extensometer. Averages of three different measurements were taken as the tensile properties of the samples. The yield strength (σ_{ys}) of the samples was calculated using the 2% offset method, and the Young's modulus (E) was obtained by calculating the slope of the linear portion of the stress-strain curves. The elastic energy of the samples was obtained by calculating the area of the elastic region under the stress-strain curves, and the toughness value was obtained by calculating the total area under the tensile curve. Field-emission SEM (ZEISS SUPRA 40 VP) was used for examining the fracture surfaces of the samples after tensile testing.

2.3. Statistical analysis

The one-way ANOVA method was used for analyzing the mechanical properties of the TZN alloy samples. Tukey's HSD post hoc test was used for determining that there were no statistically significant differences between the groups. The differences between the samples were accepted as statistically significant in cases where $\rho < 0.05$.

3. Results and discussion

3.1. Microstructures of TZN alloy samples

Fig. 2 shows the optical micrographs of the TZN alloy samples after the different thermomechanical processing steps. It can be seen that the TZN-R sample showed a fine, equiaxed grain structure after recrystallization annealing (Fig. 2f). The grain size of the TZN-S and TZN-R samples was measured as ~800 μm and ~80 μm, respectively. As can be seen from the OM images of the TZN samples after cold rolling at different reduction ratio (TZN-A, TZN-B, TZN-C, and TZN-D), different deformation products were observed in the microstructures. The deformation of grain structures increased with an increase in the cold-rolling reduction ratio. To further identify the deformation products of the TZN samples after cold rolling, EBSD analysis was carried out to determine the deformation products and therefore, the deformation mechanisms, these results are discussed later in the paper.

Fig. 3 presents the XRD patterns of the TZN alloy samples after the different thermomechanical processing steps. The TZN-S and TZN-R samples exhibit peaks only for a β phase. Ti alloys with a sufficient content of a β stabilizing element may remain in a metastable state after quenching since their martensite transformation start temperature is below room temperature. Both TZN-S and TZN-R are in an as-quenched state.

All the cold-rolled samples (TZN-A to TZN-D) exhibited peaks of a deformation-induced α" phase in addition to peaks of a β phase. Previous researches [13,14,18,22,23,27–29] has demonstrated that for some Ti alloys, transformation from the β phase to α" martensite can take place by applying stress at room temperature for some Ti alloys when the martensite start temperature is below room temperature. This deformation-induced α" phase forms as a result of the transformation of the metastable body-centered cubic (BCC) β phase into an orthorhombic crystal structure due to deformation [30]. The α" phase peaks disappeared in the XRD pattern of TZN-R, indicating that the deformation-induced α" phase transformed into a β phase. In addition, it can be seen that the width of the diffraction peaks of TZN-R decreased as compared to those of the cold-rolled TZN samples due to the release of the residual stress, similar to the results reported elsewhere [13,14].

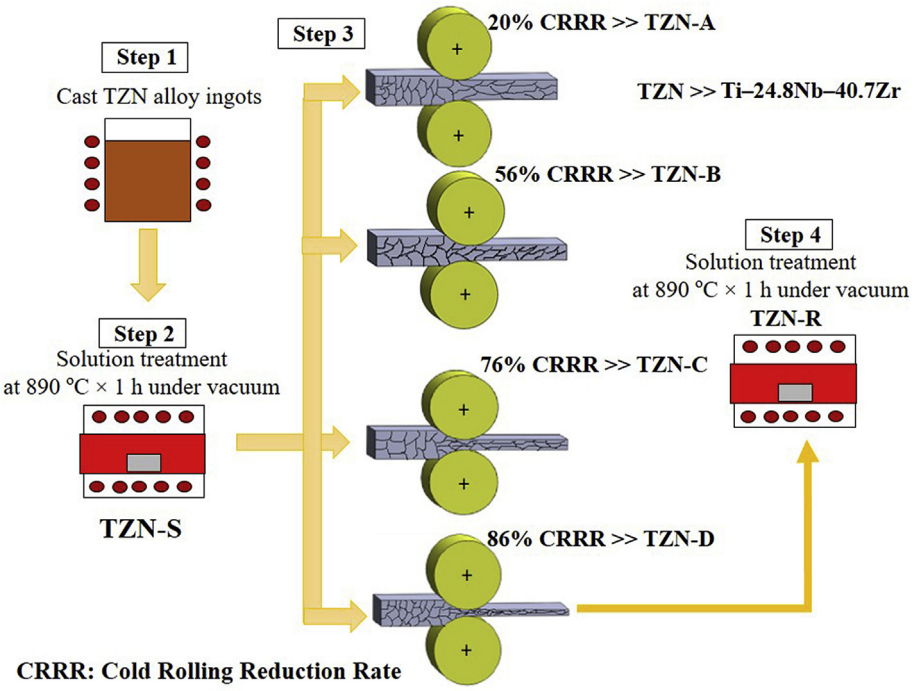

Fig. 1. Thermomechanical processing steps for Ti-40.7Zr–24.8Nb (TZN) alloy samples.

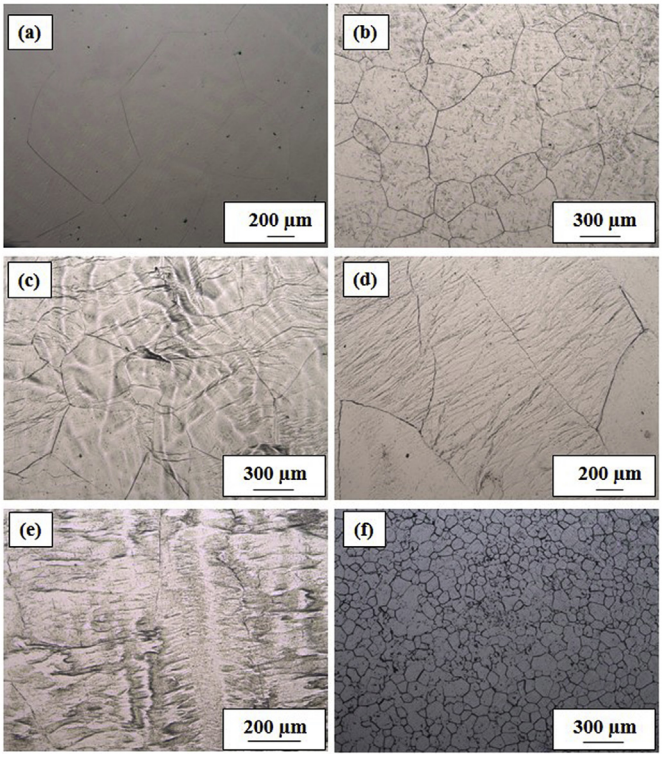

Fig. 2. Optical micrographs of TZN alloy samples: (a) TZN-S; (b) TZN-A; (c) TZN-B; (d) TZN-C; (e) TZN-D; and (f) TZN-R.

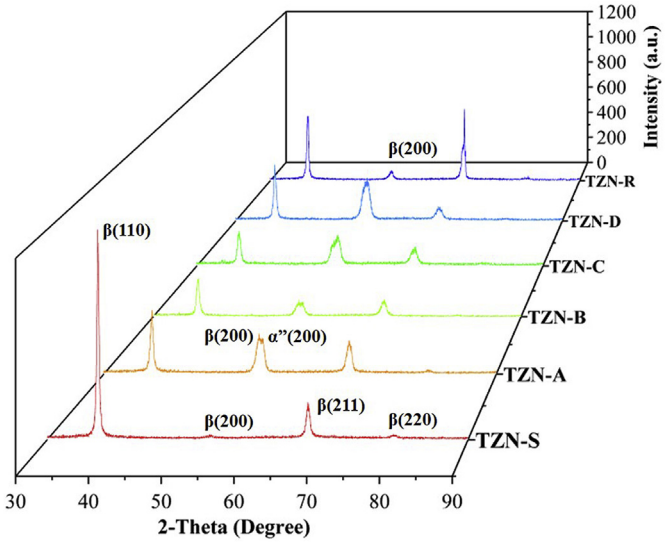

Fig. 3. XRD diffraction patterns of the TZN samples after different thermo-mechanical processing steps.

3.2. Deformation mechanisms of TZN alloy samples

Fig. 4 shows the corresponding misorientation profiles of the features in TZN-A as analyzed by EBSD. It can be seen that the β matrix and deformation products had different colors with band-type deformation products. The misorientation angles between the band formations and the β matrix were measured in order to determine the types of deformation products. Eight different misorientation profiles were drawn up based on the deformation products, marked with white arrows and it can be seen that the misorientation angles between all the deformation products and the β matrix were measured in the range of 10–30°. It has been reported that the deformation products are kink bands when the misorientation angle between the deformation product and the β matrix is between 10 and 30° [13,14,31]. In this study, the thickness of TZN-A was decreased by 20% via cold rolling and the plastic deformation resulted in the formation of kink bands. It is worth noting that kink band formation is not as common as plastic deformation mechanisms of slipping and twinning; however it is considered to be an important plastic deformation mechanism in metallic materials exhibiting strong plastic anisotropy, especially in metals and alloys with hcp crystal structure [32]. However, kink band formation has also been reported occurring during the plastic deformation of β titanium alloys

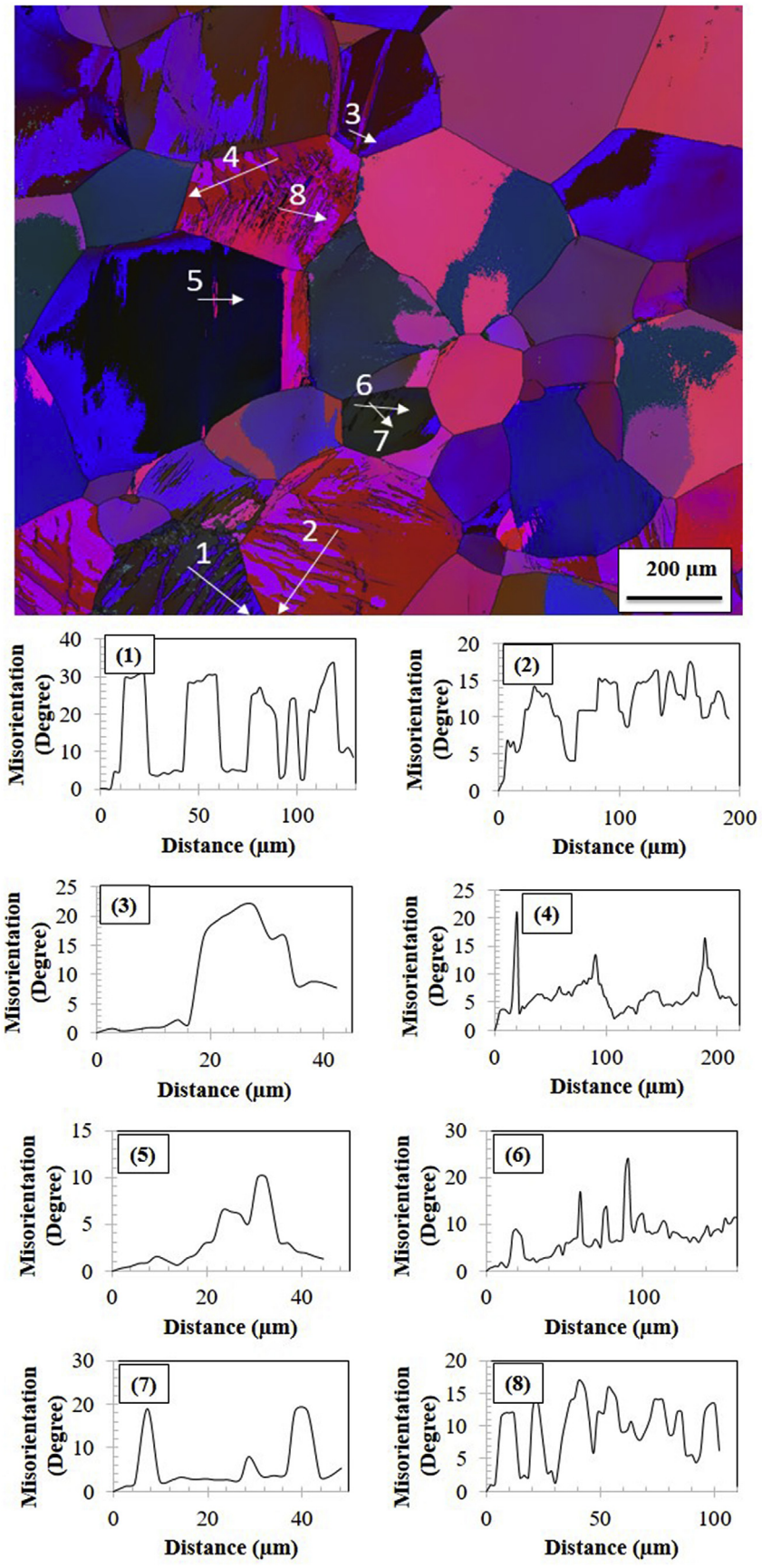

Fig. 4. Corresponding misorientation profiles of the features in TZN-A.

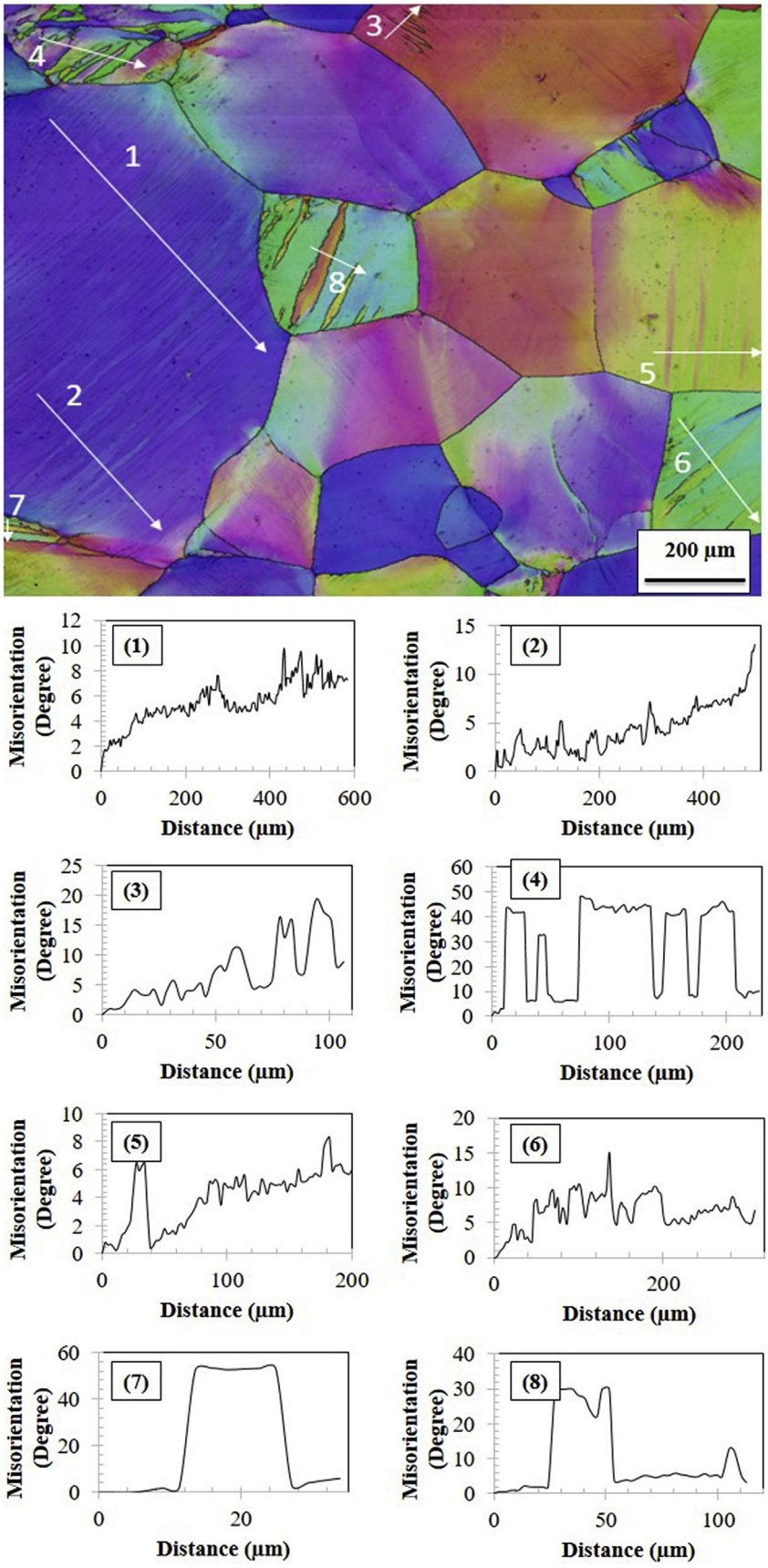

Fig. 5. Corresponding misorientation profiles of the features in TZN-B.

with bcc crystal structure [13,14,31–36]. Kink bands, which are defined as local crystallographic bands with an arbitrary degree of rotation, improve the crystal deformability of β titanium alloys during plastic deformation [31,37].

The corresponding misorientation profiles of the features in TZN-B as analyzed by EBSD are shown in Fig. 5 analyzed by EBSD. It can be seen that the misorientation angles against distance along the misorientation profiles were measured as less than 30° for the deformation products marked with the white arrows 1, 2, 3, 5, 6, and 8, indicating that these deformation products were kink bands. However, the misorientation angle against distance along the misorientation profile was measured as approximately 50.5°. It can be deduced that these deformation products were {3 3 2} < 113 > β mechanical twins along the < 110 > direction in the β matrix, as reported in previous studies [13,14,38].

The misorientation angle for the deformation product marked 4 was measured as varying between 45 and 50°. It is worth noting that the misorientation angle between the {3 3 2} < 113 > β mechanical twin and the β matrix might be lower than 50.5° in the case of a high deformation ratio, as also reported in previous studies [13,14,31]. Therefore, it can be concluded that the deformation products marked 4 were {3 3 2} < 113 > mechanical twins.

3.3. Mechanical properties of TZN alloy samples

The micro-hardness values of the TZN alloy samples after the different thermomechanical processing steps were 229.2 HV for TZN-S, 246.2 HV for TZN-R, 248.7 HV for TZN-A, 264.2 HV for TZN-B, 267.3 HV for TZN-C, and 276.7 HV for TZN-D, respectively. Unsurprisingly, the TZN alloy samples after cold rolling showed higher micro-hardnesses than those without cold rolling, and the micro-hardness increased with an increase of the reduction ratio of cold rolling. This is because the dislocation density and tangles and grain size of the samples increased with an increase in the reduction ratio of cold rolling. Also, TZN-R showed a higher micro-hardness than that of TZN-S due to its finer grain size.

Fig. 6 shows the tensile stress-strain curves of the TZN alloy samples. The tensile strength (σ_{ts}), yield strength (σ_{ys}), elongation at rupture (ε), Young's modulus (E), and elastic admissible strain (δ) values for the TZN alloy samples are given in Table 1. It can be seen that the tensile strength ranked in decreasing order was TZN-D > TZN-C > TZN-B > TZN-A > TZN-R > TZN-S. The elongation at rupture values for the TZN alloy samples were ranged from 7% to 20%, which is higher than or comparable to those of commercially available biomedical Ti alloys; for instance, the β-type Ti alloys Tiadyne 1610 (aged) [39] and Ti-35.3Nb-5.1Ta-7.1Zr (annealed) [40], α + β-type Ti alloys Ti–6Al–4V ELI (mill annealed) [39] and Ti–6Al–4V (as-cast) [41], and α-type commercially pure Ti (CP–Ti) (Grade 4) [40] exhibit an elongation at rupture of 10%, 19%, 10–15%, 8%, and 15%, respectively. It is worth noting that the elongation at rupture of the TZN Ti alloy samples decreased after cold rolling but significantly increased after recrystallization annealing and the TZN-R alloy sample showed an elongation at rupture of 20%, higher than that of all the above-mentioned alloys and the highest among all the TZN alloy samples.

Resilience is the ability of a metal to release the energy it has absorbed under elastic deformation upon unloading of the stress applied; this is measured as the modulus of resilience or elastic energy [42]. On the other hand, toughness is the energy absorbed by a metal before it is ruptured [42]. The elastic energies and toughness values of the TZN alloy samples obtained by calculating the areas of the elastic region and before rupture from their tensile curves are presented in Fig. 7. It can be seen that the elastic energy of the cold-rolled samples ranked in decreasing order was TZN-D > TZN-C > TZN-B > TZN-A. TZN-S and TZN-R showed similar elastic energies. Also, TZN-R showed the highest toughness among all the TZN alloy samples. The toughness of the TZN-R sample was drastically improved due to the refining of grain size and decreasing of location density after recrystallization annealing.

The Young's modulus of the TZN alloy samples was 63, 66, 71, 71, 72, and 72 GPa for TZN-S, TZN-R, TZN-B, TZN-C, TZN-D, and TZN-A, respectively. It is worth noting that there was no statistically significant difference ($\rho > 0.05$) between the Young's modulus values of the cold-rolled TZN alloy samples. Stress-induced ω and α" phases are likely to occur during cold rolling process of metastable titanium alloys as reported elsewhere [13,14]. It is considered that the stress-induced ω phase caused an increase in the Young's modulus of the specimens after cold rolling. It is worth noting that the Young's modulus of the stress-induced ω phase is higher than those of the stress-induced α" and β phases [43,44]. In this study, the effect of stress-induced ω phase on the Young's modulus of the specimens may be more dominant than the Young's modulus lowering effect of the stress-induced α" phase, leading to an overall increase in the Young's modulus of the specimens.

These Young's modulus values are promising in terms of orthopedic implant applications because they are significantly lower than those of CP-Ti and Ti–6Al–4V, the most widely used biomedical Ti alloys. High mechanical strength coupled with low Young's modulus are highly desirable for orthopedic implant applications [12–14,45,46]. The biomechanical compatibility of orthopedic implant materials is evaluated via the elastic admissible strain, which is calculated by dividing the yield strength by the Young's modulus of the materials ($\delta = \sigma_{ys}/E$). It is possible to compare various orthopedic implant materials with regard to their biomechanical compatibility by using δ [8,9,12]. A higher δ means a more biomechanically compatible material [12,46]. The elastic admissible strain of the TZN alloy samples was 0.97%, 1.18%, 1.22%, 1.22%, 1.43%, and 1.47% for TZN-A, TZN-S, TZN-R, TZN-B, TZN-C, and TZN-D, respectively (Table 1). It is worth noting that TZN-D exhibited the highest elastic admissible strain among all the TZN alloy samples and its value of δ = 1.47% was considerably higher than those of the as-cast alloy (δ = 1.08%) [12], CP-Ti (δ = 0.47%) [40] and Ti–6Al–4V (δ = 0.80%) [39]. It is possible to obtain structural and functional Ti alloys with excellent mechanical performance via severe plastic deformation [13,14,21,38,47,48]. In this study, TZN-D after cold rolling at an 86% reduction ratio exhibited a yield strength of 1061 MPa, a tensile strength of 1158 MPa, a Young's modulus of 72 GPa, and an ultrahigh elastic admissible strain of 1.47%.

The tensile fracture surfaces of the TZN alloy samples are shown in Fig. 8. It can be seen that all the TZN alloy samples exhibited the ductile fracture characteristics of dimples, but the dimples on the fracture surface of TZN-R were larger and deeper than those of the cold-rolled samples of TZN-A, TZN-B, TZN-C, and TZN-D, and the solution treated sample of TZN-S. Following the neck formation in the specimen, separation of the inclusions from the rest of the material and/or fracture of the inclusions result in microvoid formations [49]. With advancing deformation, those microvoids grow and coalesce, causing cracks to occur in the material [50]. The formation of cracks continues to grow as those microvoids coalesce [42,50]. Finally, following the rapid crack propagation, fracture occurs [42,50]. Since one of the fractured pieces resembles a cup and the other is a cone, this kind of fracture is called a cup-and-cone type fracture [42]. The ductile cup-and-cone type fracture morphology shown in TZN-R was formed due to the microvoid coalescence mechanism. In addition, cleavage formation combined with shallow vein patterns were observed on the fracture surfaces of the cold-rolled TZN alloy samples.

4. Conclusions

The microstructure, deformation mechanisms, tensile and microhardness properties of thermomechanically processed TZN alloy samples were investigated. The main conclusions are as follows:

a Deformation of the TZN alloy samples during cold rolling occurred via kink band formation, {3 3 2} < 113 > mechanical twinning, and stress-induced α" formation. All the deformation products were

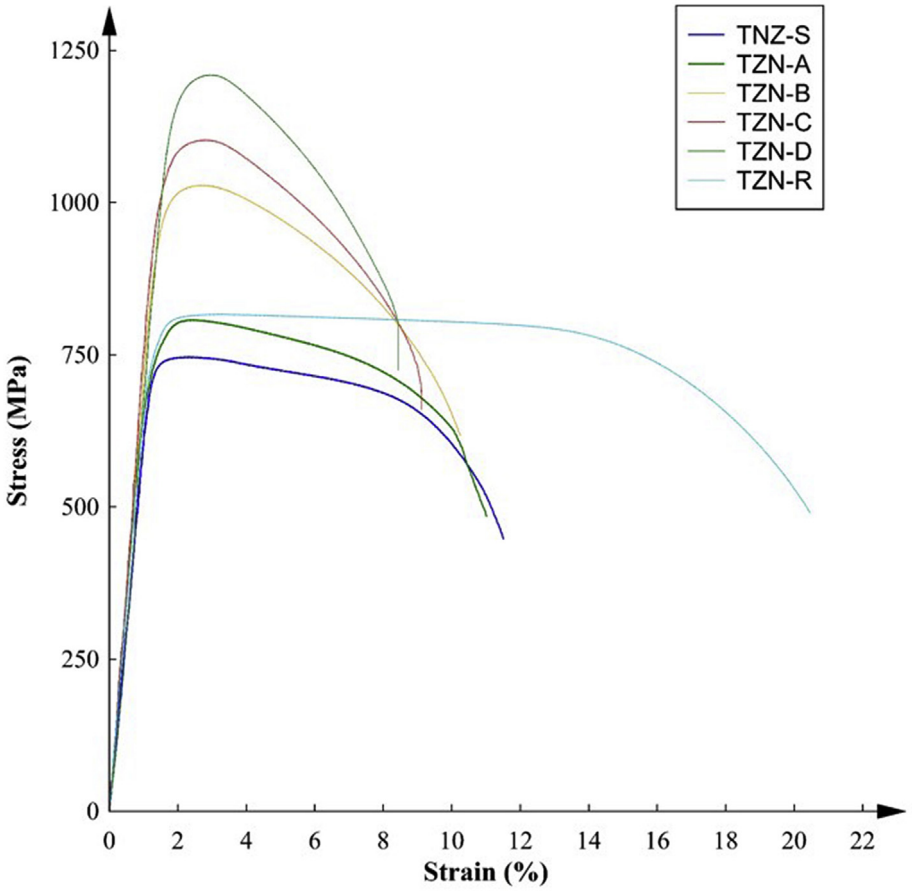

Fig. 6. Tensile stress-strain curves of TZN alloy samples.

disappeared after recrystallization annealing, resulting in the formation of a fine, equiaxed single β phase.

b The TZN alloy samples showed higher tensile strength, Young's modulus and micro-hardness values after cold rolling. The TZN alloy after cold rolling at an 86% reduction ratio showed 7% elongation at rupture, 1061 MPa yield strength, 1158 MPa tensile strength, 72 GPa Young's modulus, and 1.47% elastic admissible strain; and for the alloy sample after recrystallization annealing showed 20% elongation at rupture, 803 MPa yield strength, 848 MPa tensile strength, 66 GPa Young's modulus, and 1.22% elastic admissible strain.

c All the TZN alloy samples after the various thermomechanical processes exhibited elongation at rupture ranging from 7% to 20%, which is higher than or comparable to those of the commercially available medical Ti alloys.

d The tensile fracture surface of the TZN alloy sample after cold rolling at an 86% reduction ratio plus recrystallization annealing showed the ductile fracture characteristics of large and deep dimples.

e Overall, the TZN alloys with composition of Ti-40.7Zr–24.8Nb can be considered promising candidate materials for biomedical applications in terms of their high mechanical strength, cold-forming ability and high ductility.

Declaration of competing interests

The authors declare that there are no conflicts of interest.

Acknowledgements

The authors acknowledge the financial support for this research by the National Health and Medical Research Council (NHMRC), Australia, through grant GNT1087290; and the Australian Research Council (ARC) through the discovery grant DP170102557. YL is also supported through an ARC Future Fellowship (FT160100252). JL acknowledges the support for this research by Hunan Provincial Natural Science Foundation of China through the Grant 2016JC2005. The authors also acknowledge the scientific and technical assistance of RMMF (RMIT

Table 1
Tensile properties of the thermo-mechanically treated TZN alloy samples.

TZN alloy	σ_{ys} (MPa)	σ_{ts} (MPa)	E (GPa)	ε (%)	δ (%)	Phases
TZN-S	740 ± 12	753 ± 6	63 ± 2	10 ± 2	1.18 ± 0.02	β
TZN-A	692 ± 21	799 ± 12	72 ± 1	11 ± 1	0.97 ± 0.04	β + α″
TZN-B	865 ± 130	981 ± 67	71 ± 3	9 ± 2	1.22 ± 0.13	β + α″
TZN-C	1007 ± 57	1072 ± 44	71 ± 0	8 ± 1	1.43 ± 0.08	β + α″
TZN-D	1061 ± 70	1158 ± 74	72 ± 2	7 ± 3	1.47 ± 0.13	β + α″
TZN-R	803 ± 81	848 ± 44	66 ± 2	20 ± 1	1.22 ± 0.15	β

σ_{ts}: tensile strength; E: elastic modulus; ε: elongation; δ: elastic admissible strain.

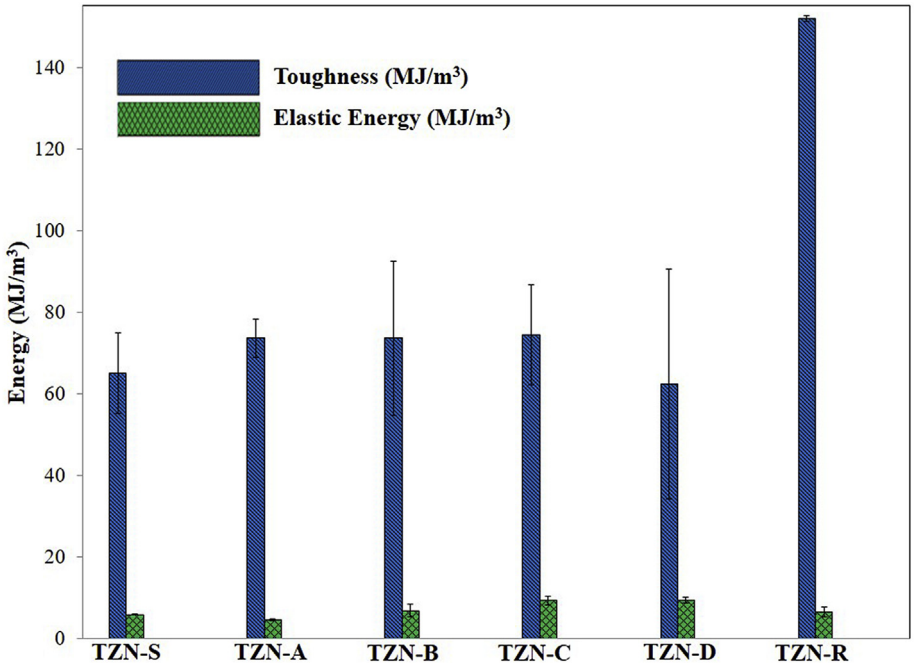

Fig. 7. Elastic energy and toughness of TZN alloy samples after different thermomechanical processing steps.

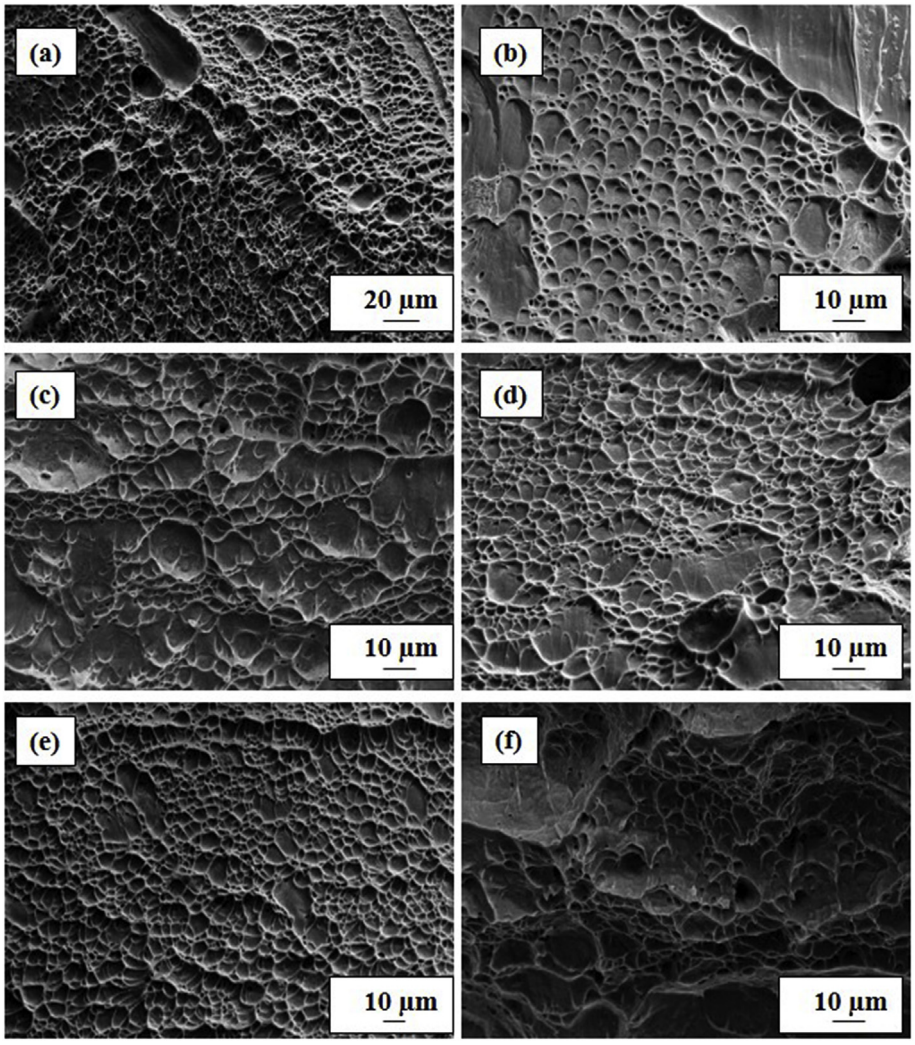

Fig. 8. Tensile fracture surfaces of: (a) TZN-S; (b) TZN-A; (c) TZN-B; (d) TZN-C; (e) TZN-D; and (f) TZN-R.

University's Microscopy and Microanalysis Facility, a linked laboratory of the Australian Microscopy & Microanalysis Research Facility).

References

[1] L.C. Biant, W.J.M. Bruce, H. van der Wall, W.R. Walsh, Infection or allergy in the painful metal-on-metal total hip arthroplasty? J. Arthroplast. 25 (2010) 334.e311–334.e316, https://doi.org/10.1016/j.arth.2008.08.015.

[2] M. Zhubrak, T. Bar-David, Systemic nickel allergy after internal fixation of a bunionectomy, J. Foot Ankle Surg. 53 (2014) 466–467, https://doi.org/10.1053/j.jfas.2014.03.006.

[3] S.B. Sesia, F.-M. Haecker, B. Shah, M.J. Goretsky, R.E. Kelly, R.J. Obermeyer, Development of metal allergy after Nuss procedure for repair of pectus excavatum despite preoperative negative skin test, J. Pediatr. Surg. Case Rep. 1 (2013) 152–155, https://doi.org/10.1016/j.epsc.2013.05.004.

[4] M. Hosoki, K. Nishigawa, Y. Miyamoto, G. Ohe, Y. Matsuka, Allergic contact dermatitis caused by titanium screws and dental implants, J. Prosthodont. Res. 60 (2016) 213–219, https://doi.org/10.1016/j.jpor.2015.12.004.

[5] P. Phedy, Y.P. Djaja, D.R. Boedijono, M. Wahyudi, J. Silitonga, I. Solichin, Hypersensitivity to orthopaedic implant manifested as erythroderma: timing of implant removal, Int. J. Surg. Case Rep. 49 (2018) 110–114, https://doi.org/10.1016/j.ijscr.2018.06.011.

[6] M.F. Saccomanno, G. Sircana, G. Masci, G. Cazzato, M. Florio, L. Capasso, M. Passiatore, G. Autore, G. Maccauro, E. Pola, Allergy in total knee replacement surgery: is it a real problem? World J. Orthop. 10 (2019) 63–70, https://doi.org/10.5312/wjo.v10.i2.63.

[7] M. Geetha, A.K. Singh, R. Asokamani, A.K. Gogia, Ti based biomaterials, the ultimate choice for orthopaedic implants – a review, Prog. Mater. Sci. 54 (2009) 397–425, https://doi.org/10.1016/j.pmatsci.2008.06.004.

[8] M. Abdel-Hady Gepreel, M. Niinomi, Biocompatibility of Ti-alloys for long-term implantation, J. Mech. Behav. Biomed. Mater. 20 (2013) 407–415, https://doi.org/10.1016/j.jmbbm.2012.11.014.

[9] Y. Song, D.S. Xu, R. Yang, D. Li, W.T. Wu, Z.X. Guo, Theoretical study of the effects of alloying elements on the strength and modulus of β-type bio-titanium alloys, Mater. Sci. Eng. A 260 (1999) 269–274, https://doi.org/10.1016/S0921-5093(98)00886-7.

[10] R. Huiskes, H. Weinans, B. Vanrietbergen, The relationship between stress shielding and bone-resorption around total hip stems and the effects of flexible materials, Clin. Orthop. Relat. Res. (1992) 124–134.

[11] P. Heinl, A. Rottmair, C. Korner, R.F. Singer, Cellular titanium by selective electron beam melting, Adv. Eng. Mater. 9 (2007) 360–364, https://doi.org/10.1002/adem.200700025.

[12] S. Ozan, J. Lin, Y. Li, R. Ipek, C. Wen, Development of Ti–Nb–Zr alloys with high elastic admissible strain for temporary orthopedic devices, Acta Biomater. 20 (2015) 176–187, https://doi.org/10.1016/j.actbio.2015.03.023.

[13] S. Ozan, Y. Li, J. Lin, Y. Zhang, H. Jiang, C. Wen, Microstructural evolution and its influence on the mechanical properties of a thermomechanically processed β Ti–32Zr–30Nb alloy, Mater. Sci. Eng. A 719 (2018) 112–123, https://doi.org/10.1016/j.msea.2018.02.034.

[14] S. Ozan, J. Lin, Y. Li, Y. Zhang, K. Munir, H. Jiang, C. Wen, Deformation mechanism and mechanical properties of a thermomechanically processed β Ti–28Nb–35.4Zr alloy, J. Mech. Behav. Biomed. Mater. 78 (2018) 224–234, https://doi.org/10.1016/j.jmbbm.2017.11.025.

[15] H. Matsumoto, S. Watanabe, S. Hanada, α′ Martensite Ti–V–Sn alloys with low Young's modulus and high strength, Mater. Sci. Eng. A 448 (2007) 39–48, https://doi.org/10.1016/j.msea.2006.11.022.

[16] H. Matsumoto, S. Watanabe, S. Hanada, Microstructures and mechanical properties of metastable β TiNbSn alloys cold rolled and heat treated, J. Alloy. Comp. 439 (2007) 146–155, https://doi.org/10.1016/j.jallcom.2006.08.267.

[17] S. Dai, Y. Wang, F. Chen, X. Yu, Y. Zhang, Effects of cold deformation on microstructure and mechanical properties of Ti–35Nb–9Zr–6Mo–4Sn alloy for biomedical applications, Mater. Sci. Eng. A 575 (2013) 35–40, https://doi.org/10.1016/j.msea.2013.03.032.

[18] G. Choi, K. Lee, Effect of cold rolling on the microstructural evolution of new β-typed Ti–6Mo–6V–5Cr–3Sn–2.5Zr alloys, Mater. Char. 123 (2017) 67–74, https://doi.org/10.1016/j.matchar.2016.11.007.

[19] S.J. Li, M.T. Jia, F. Prima, Y.L. Hao, R. Yang, Improvements in nonlinear elasticity and strength by grain refinement in a titanium alloy with high oxygen content, Scr. Mater. 64 (2011) 1015–1018, https://doi.org/10.1016/j.scriptamat.2011.02.006.

[20] Y.L. Hao, Z.B. Zhang, S.J. Li, R. Yang, Microstructure and mechanical behavior of a Ti–24Nb–4Zr–8Sn alloy processed by warm swaging and warm rolling, Acta Mater. 60 (2012) 2169–2177, https://doi.org/10.1016/j.actamat.2012.01.003.

[21] L. Wang, W. Lu, J. Qin, F. Zhang, D. Zhang, Microstructure and mechanical properties of cold-rolled TiNbTaZr biomedical β titanium alloy, Mater. Sci. Eng. A 490 (2008) 421–426, https://doi.org/10.1016/j.msea.2008.03.003.

[22] S. Hanada, N. Masahashi, T.K. Jung, M. Miyake, Y.S. Sato, H. Kokawa, Effect of swaging on Young's modulus of β Ti–33.6Nb–4Sn alloy, J. Mech. Behav. Biomed. Mater. 32 (2014) 310–320, https://doi.org/10.1016/j.jmbbm.2013.10.027.

[23] S. Hanada, N. Masahashi, T.K. Jung, Effect of stress-induced α″ martensite on Young's modulus of β Ti–33.6Nb–4Sn alloy, Mater. Sci. Eng. A 588 (2013) 403–410, https://doi.org/10.1016/j.msea.2013.09.053.

[24] X. Zhao, M. Niinomi, M. Nakai, T. Ishimoto, T. Nakano, Development of high Zr-containing Ti-based alloys with low Young's modulus for use in removable implants, Mater. Sci. Eng. C 31 (2011) 1436–1444, https://doi.org/10.1016/j.msec.2011.05.013.

[25] E. Kobayashi, M. Ando, Y. Tsutsumi, H. Doi, T. Yoneyama, M. Kobayashi, T. Hanawa, Inhibition effect of zirconium coating on calcium phosphate precipitation of titanium to avoid assimilation with bone, Mater. Trans. 48 (2007) 301–306, https://doi.org/10.2320/matertrans.48.301.

[26] T. Hanawa, O. Okuno, H. Hamanaka, Compositional change in surface of Ti-Zr alloys in artificial bioliquid, J. Jpn. Inst. Metals 56 (1992) 1168–1173, https://doi.org/10.2320/jinstmet1952.56.10_1168.

[27] S. Sadeghpour, S.M. Abbasi, M. Morakabati, Deformation-induced martensitic transformation in a new metastable β titanium alloy, J. Alloy. Comp. 650 (2015) 22–29, https://doi.org/10.1016/j.jallcom.2015.07.263.

[28] X. Ma, F. Li, X. Fang, Z. Li, Z. Sun, J. Hou, J. Cao, Effect of strain reversal on the stress-induced martensitic transformation and tensile properties of a metastable β titanium alloy, J. Alloy. Comp. 784 (2019) 111–116, https://doi.org/10.1016/j.jallcom.2019.01.010.

[29] S. Neelakantan, E.I. Galindo-Nava, D. San Martin, J. Chao, P.E.J. Rivera-Díaz-del-Castillo, Modelling and design of stress-induced martensite formation in metastable β Ti alloys, Mater. Sci. Eng. A 590 (2014) 140–146, https://doi.org/10.1016/j.msea.2013.10.003.

[30] T. Grosdidier, C. Roubaud, M.-J. Philippe, Y. Combres, The deformation mechanisms in the β-metastable β-Cez titanium alloy, Scr. Mater. 36 (1997) 21–28, https://doi.org/10.1016/S1359-6462(96)00341-7.

[31] Y. Yang, S.Q. Wu, G.P. Li, Y.L. Li, Y.F. Lu, K. Yang, P. Ge, Evolution of deformation mechanisms of Ti–22.4Nb–0.73Ta–2Zr–1.34O alloy during straining, Acta Mater. 58 (2010) 2778–2787, https://doi.org/10.1016/j.actamat.2010.01.015.

[32] Y. Zheng, W. Zeng, Y. Wang, S. Zhang, Kink deformation in a beta titanium alloy at high strain rate, Mater. Sci. Eng. A 702 (2017) 218–224, https://doi.org/10.1016/j.msea.2017.07.015.

[33] Y. Zheng, W. Zeng, Y. Wang, D. Zhou, X. Gao, High strain rate compression behavior of a heavily stabilized beta titanium alloy: kink deformation and adiabatic shearing, J. Alloy. Comp. 708 (2017) 84–92, https://doi.org/10.1016/j.jallcom.2017.02.284.

[34] S. Sadeghpour, S.M. Abbasi, M. Morakabati, A. Kisko, L.P. Karjalainen, D.A. Porter, On the compressive deformation behavior of new beta titanium alloys designed by d-electron method, J. Alloy. Comp. 746 (2018) 206–217, https://doi.org/10.1016/j.jallcom.2018.02.212.

[35] H. Liu, M. Niinomi, M. Nakai, K. Cho, K. Narita, M. Şen, H. Shiku, T. Matsue, Mechanical properties and cytocompatibility of oxygen-modified β-type Ti–Cr alloys for spinal fixation devices, Acta Biomater. 12 (2015) 352–361, https://doi.org/10.1016/j.actbio.2014.10.014.

[36] H. Liu, M. Niinomi, M. Nakai, J. Hieda, K. Cho, Deformation-induced changeable Young's modulus with high strength in β-type Ti–Cr–O alloys for spinal fixture, J. Mech. Behav. Biomed. Mater. 30 (2014) 205–213, https://doi.org/10.1016/j.jmbbm.2013.11.001.

[37] T. Sakai, H. Miura, X. Yang, Ultrafine grain formation in face centered cubic metals during severe plastic deformation, Mater. Sci. Eng. A 499 (2009) 2–6, https://doi.org/10.1016/j.msea.2007.11.098.

[38] T. Furuta, S. Kuramoto, J. Hwang, K. Nishino, T. Saito, Elastic deformation behavior of multi-functional Ti-Nb-Ta-Zr-O alloys, Mater. Trans. 46 (2005) 3001–3007, https://doi.org/10.2320/matertrans.46.3001.

[39] K. Wang, The use of titanium for medical applications in the USA, Mater. Sci. Eng. A 213 (1996) 134–137, https://doi.org/10.1016/0921-5093(96)10243-4.

[40] M. Niinomi, Mechanical properties of biomedical titanium alloys, Mater. Sci. Eng. A 243 (1998) 231–236, https://doi.org/10.1016/S0921-5093(97)00806-X.

[41] ASTM, ASTM F1108-04. Standard Specification for Titanium-6 aluminum-4 vanadium Alloy Castings for Surgical Implants (UNS R56406), ASTM International, West Conshohocken, PA, 2004.

[42] W.D. Callister, Materials Science and Engineering: an Introduction, seventh ed., John Wiley and Sons, New York, 2007.

[43] M. Niinomi, T. Hattori, K. Morikawa, T. Kasuga, A. Suzuki, H. Fukui, S. Niwa, Development of low rigidity β-type titanium alloy for biomedical applications, Mater. Trans. 43 (2002) 2970–2977, https://doi.org/10.2320/matertrans.43.2970.

[44] Y.L. Hao, R. Yang, M. Niinomi, D. Kuroda, Y.L. Zhou, K. Fukunaga, A. Suzuki, Aging response of the young's modulus and mechanical properties of Ti-29Nb-13Ta-4.6Zr for biomedical applications, Metall. Mater. Trans. A 34 (2003) 1007–1012, https://doi.org/10.1007/s11661-003-0230-x.

[45] S. Ozan, J. Lin, Y. Li, C. Wen, New Ti-Ta-Zr-Nb alloys with ultrahigh strength for potential orthopedic implant applications, J. Mech. Behav. Biomed. Mater. 75 (2017) 119–127, https://doi.org/10.1016/j.jmbbm.2017.07.011.

[46] A. Biesiekierski, J. Lin, K. Munir, S. Ozan, Y. Li, C. Wen, An investigation of the mechanical and microstructural evolution of a TiNbZr alloy with varied ageing time, Sci. Rep. 8 (2018) 5737, https://doi.org/10.1038/s41598-018-24155-y.

[47] G.S. Zhang, Q. Zhang, K.F. Li, Y.B. Cao, M. Li, W.K. Shan, D.F. Guo, Tailoring elastic admissible strain of TiZr alloy by cold rolling deformation, J. Alloy. Comp. 781 (2019) 504–507, https://doi.org/10.1016/j.jallcom.2018.11.388.

[48] V.N. Chuvil'deev, V.I. Kopylov, A.V. Nokhrin, P.V. Tryaev, N.Y. Tabachkova, M.K. Chegurov, N.A. Kozlova, A.S. Mikhaylov, A.V. Ershova, M.Y. Grayznov, I.S. Shadrina, C.V. Likhnitskii, Effect of severe plastic deformation realized by rotary swaging on the mechanical properties and corrosion resistance of near-α-titanium alloy Ti-2.5Al-2.6Zr, J. Alloy. Comp. 785 (2019) 1233–1244, https://doi.org/10.1016/j.jallcom.2019.01.268.

[49] F. Suárez, J.C. Gálvez, D.A. Cendón, J.M. Atienza, Fracture of eutectoid steel bars under tensile loading: experimental results and numerical simulation, Eng. Fract. Mech. 158 (2016) 87–105, https://doi.org/10.1016/j.engfracmech.2016.02.044.

[50] T.L. Anderson, Fracture Mechanics: Fundamentals and Applications, third ed., CRC press, Boca Raton, 2005.